AFRL-RX-WP-TP-2012-0217

EFFECT OF SPECIMEN THICKNESS ON THE CREEP RESPONSE OF A SINGLE CRYSTAL SUPERALLOY (PREPRINT)

A. Srivastava, S. Gopagoni, A. Needleman, and R. Banerjee
University of North Texas

V. Seetharaman and A. Staroselsky
Prat & Whitney

JANUARY 2012

AIR FORCE RESEARCH LABORATORY
MATERIALS AND MANUFACTURING DIRECTORATE
WRIGHT-PATTERSON AIR FORCE BASE, OH 45433-7750
AIR FORCE MATERIEL COMMAND
UNITED STATES AIR FORCE

NOTICE AND SIGNATURE PAGE

Using Government drawings, specifications, or other data included in this document for any purpose other than Government procurement does not in any way obligate the U.S. Government. The fact that the Government formulated or supplied the drawings, specifications, or other data does not license the holder or any other person or corporation; or convey any rights or permission to manufacture, use, or sell any patented invention that may relate to them.

This report was cleared for public release by the USAF 88th Air Base Wing (88 ABW) Public Affairs Office and is available to the general public, including foreign nationals. Copies may be obtained from the Defense Technical Information Center (DTIC) (http://www.dtic.mil).

AFRL-RX-WP-TR-2012-0217 HAS BEEN REVIEWED AND IS APPROVED FOR PUBLICATION IN ACCORDANCE WITH ASSIGNED DISTRIBUTION STATEMENT.

//SIGNED//

JAY TILEY, Program Manager
Metals Branch
Metals, Ceramics & Nondestructive Evaluation Division

//SIGNED//

BRANCH CHIEF, Chief
Metals Branch
Metals, Ceramics & Nondestructive Evaluation Division

//SIGNED//

DIVISION CHIEF, Division Chief
Metals, Ceramics & Nondestructive Evaluation Division
Materials and Manufacturing Directorate

This report is published in the interest of scientific and technical information exchange, and its publication does not constitute the Government's approval or disapproval of its ideas or findings.

*Disseminated copies will show "//signature//" stamped or typed above the signature blocks.

REPORT DOCUMENTATION PAGE

Form Approved
OMB No. 0704-0188

1. REPORT DATE *(DD-MM-YY)*	2. REPORT TYPE	3. DATES COVERED *(From - To)*
January 2012	Technical Paper	1 November 2011 – 1 November 2011

4. TITLE AND SUBTITLE

EFFECT OF SPECIMEN THICKNESS ON THE CREEP RESPONSE OF A SINGLE CRYSTAL SUPERALLOY (PREPRINT)

5a. CONTRACT NUMBER
FA8650-08-C-5226

5b. GRANT NUMBER

5c. PROGRAM ELEMENT NUMBER
62102F

6. AUTHOR(S)

A. Srivastava, S. Gopagoni, A. Needleman, and R. Banerjee (University of North Texas)
V. Seetharaman and A. Staroselsky (Prat & Whitney)

5d. PROJECT NUMBER
4347

5e. TASK NUMBER
0

5f. WORK UNIT NUMBER
LM114100

7. PERFORMING ORGANIZATION NAME(S) AND ADDRESS(ES)

University of North Texas
Corner of Ave. C Chestnut
Denten, TX 76203

Pratt & Whitney

8. PERFORMING ORGANIZATION REPORT NUMBER
AFRL-RX-WP-TP-2012-0217

9. SPONSORING/MONITORING AGENCY NAME(S) AND ADDRESS(ES)

Air Force Research Laboratory
Materials and Manufacturing Directorate
Wright-Patterson Air Force Base, OH 45433-7750
Air Force Materiel Command
United States Air Force

10. SPONSORING/MONITORING AGENCY ACRONYM(S)
AFRL/RXLM

11. SPONSORING/MONITORING AGENCY REPORT NUMBER(S)
AFRL-RX-WP-TP-2012-0217

12. DISTRIBUTION/AVAILABILITY STATEMENT

Approved for public release; distribution unlimited.

13. SUPPLEMENTARY NOTES

The U.S. Government is joint author of this work and has the right to use, modify, reproduce, release, perform, display, or disclose the work. PA Case Number and clearance date: 88ABW-2011-6138, 28 Nov 2011. Preprint journal article to be submitted to Acta Materialia. This document contains color.

14. ABSTRACT

Creep tests on single crystal superalloy sheet specimens have shown a thickness dependent creep behavior. This is termed the thickness debit effect. To investigate the mechanism of thickness debit effect, isothermal, constant nominal stress creep tests at two test conditions 760◦C/758MPa and 982◦C/248MPa were performed on the uncoated sheet specimens of thicknesses 3.18mm and 0.51mm of PWA1484 Ni-base single crystal superalloy. It was observed that the dependence on specimen thickness under the two test conditions are different. At 760◦C/758MPa reduction in creep strain to rupture with decreasing section

15. SUBJECT TERMS

creep, creep rupture, thickness debit effect, superalloy, PWA1484, single crystal, oxidation, recrystallization

16. SECURITY CLASSIFICATION OF:			17. LIMITATION OF ABSTRACT:	NUMBER OF PAGES	19a. NAME OF RESPONSIBLE PERSON (Monitor)
a. REPORT	b. ABSTRACT	c. THIS PAGE			Jay Tiley
Unclassified	Unclassified	Unclassified	SAR	28	19b. TELEPHONE NUMBER *(Include Area Code)* N/A

Effect of specimen thickness on the creep response of a single crystal superalloy

A. Srivastava[1], S. Gopagoni[1], A. Needleman[1], V. Seetharaman[2], A. Staroselsky[2], R. Banerjee[1]

[1]*Department of Materials Science and Engineering, University of North Texas, Denton, TX, USA*
[2]*Pratt & Whitney,* 400 *Main Street, East Hartford, CT* 06108*, USA*

Abstract

Creep tests on single crystal superalloy sheet specimens have shown a thickness dependent creep behavior. This is termed the thickness debit effect. To investigate the mechanism of thickness debit effect, isothermal, constant nominal stress creep tests at two test conditions 760°C/758MPa and 982°C/248MPa were performed on the uncoated sheet specimens of thicknesses 3.18mm and 0.51mm of PWA1484 Ni-base single crystal superalloy. It was observed that the dependence on specimen thickness under the two test conditions are different. At 760°C/758MPa reduction in creep strain to rupture with decreasing section thickness was observed that led to reduced creep life. At 982°C/248MPa decreasing thickness resulted in increased creep rate even at low strain levels. No trend was observed in creep strain to rupture for different thicknesses at 982°C/248MPa. The reduction in overall creep life at 982°C/248MPa was less as compared to 760°C/758MPa. Microscopic analysis revealed that the thin specimens at 760°C/758MPa failed predominantly due to cleavage and were less damage tolerant as compared to thick specimen. Specimens creep tested at 982°C/248MPa and in air showed oxidation that led to precipitate free and precipitate depletion zone. The surface cracks formed in the oxide scale were arrested by further oxidation. Thicker specimen showed dimple rupture whereas thin specimen showed a mixed mode of ductile and cleavage fracture at 982°C/248MPa.

Keywords: Creep, Creep rupture, Thickness debit effect, Superalloy, PWA1484, Single Crystal, Oxidation, Recrystallization

1. Introduction

Single crystal Ni-base superalloys were introduced in the early 80's [1], since then they have been widely used in turbine aerofoils in jet engines in order to allow for increased turbine inlet gas temperatures so as to improve thermal efficiency. The desire for weight reduction and the use of advanced metal cooling schemes to improve jet engine efficiency tends to drive designs toward thinner airfoil walls [2]. Creep tests on Ni-base superalloy specimens have shown greater creep strain rates and/or reduced creep life for thinner specimens than predicted by current theories [3–13]. This is known as the thickness debit effect.

The understanding of creep in single crystal superalloy turbine blades is of importance for designing more reliable and fuel efficient aircraft engines.

A qualitative comparison of the thickness debit effect for conventionally cast, columnar grain and single crystal PWA1483 superalloy materials by Duhl [4] showed that thickness debit effect is smallest for single crystals. Doner and Heckler [3, 5] investigated thickness debit effect in single crystal CMSX-3 mini-flat specimens. A 30% reduction in creep rupture life was found for uncoated specimens tested in air at 982°C and at a stress level below 275MPa when the thickness was reduced from 3.18 to 0.76mm. On the other hand, Doner and Heckler [3, 5] observed no thickness debit effect for both aluminide coated and uncoated specimens tested in high purity argon. Hüttner et al. [12, 13] reported thickness debit in the creep response of both coated and uncoated specimens of René N5 single crystal superalloy at a test temperature of 980°C. In their work coated samples showed higher thickness debit effect than the corresponding uncoated samples. They also showed that the samples with misorientation of about 16° showed increased thickness debit effect as compared to $< 001 >$ orientated samples. Seetharaman and Cetel [10] performed creep tests on uncoated PWA1484 (see Cetel and Duhl [17]) single crystal superalloy specimens in air at four conditions: 760°C/758MPa, 871°C/413MPa, 982°C/207MPa and 982°C/248MPa. They found a moderate thickness debit effect for the high temperature low stress (982°C/248MPa) condition and a greater thickness debit effect for the low temperature high stress (760°C/758MPa) condition.

In view of the experimental results, a variety of mechanism have been proposed as being responsible for the thickness debit effect. Baldan [8] presumed that the thickness debit effect is observed due to the damage mechanism occurring throughout the section and argued that the creep response is controlled by the crack size to section size ratio. Doner and Heckler [3, 5] suggested that the degradation in stress rupture life in their experiments was primarily due to environmental effects. Seetharaman and Cetel [10] considered several possible explanations including deformation constraint; cavity nucleation, growth and coalescence; environmental degradation; and changes in anisotropy with section thickness. Gullickson et al. [14] assumed that the thickness debit effect observed in the creep tests of Seetharaman and Cetel [10] was due to damage occurring in a surface layer. They used a constitutive model for the nucleation and growth of voids and carried out three dimensional finite element analyses incorporating a surface damage layer. Cassenti and Staroselsky [15] modeled a mechanism involving an overstressed boundary layer created due to plastic slip and the preferential generation of voids or micro-cracks near surface to explain the thickness debit effect. The results for the thickness dependence of creep curves in [14, 15] were qualitatively consistent with the experimental observations. Bensch et al. [16] analyzed surface oxidation in uncoated specimens to model the thickness debit reported in [12, 13]. Their results showed that surface oxidation could qualitatively explain the thickness debit effect where environmental degradation is an active mechanism.

Given the variety of proposed mechanisms and explanations, it is clear that the mechanism of thickness debit effect in creep properties of single crystal superalloys is not yet completely understood. Hence, to further investigate the thickness debit effect, we carried out creep tests on sheet specimens of the same material and for the two temperature/loading

conditions viz. 760°/758MPa and 982°C/248MPa as in Seetharaman and Cetel [10] for specimen thicknesses of 3.18mm and 0.51mm. Some tests were allowed to proceed until the specimens ruptured, while several were terminated at a predetermined creep strain.

2. Material description and experimental procedure

Single crystal bars (25.4mm diameter × 228.6mm long) of PWA1484 [17] alloy with nominal chemical composition of (in weight percent) Co 10.0%,Cr 5.0%, Al 5.6%, Ta 8.7%, W 6.0%, Mo 2.0%, Re 3.0%, and Ni the balance were directionally solidified at Pratt & Whitneys in-house Rapid Prototype Casting Laboratory. The X-ray diffraction (Laue) analysis and macro-etching were used to confirm that the bars were single crystals with primary orientation within 10° of [100] axis. These bars were subjected to a standard sequence of heat treatment cycles, viz., solution annealing at 1316°C (2400°F) for 2hours in vacuum, coating diffusion heat treatment at 1080°C (1975°F) for 4hours in a controlled atmosphere, and precipitation heat treatment at 704°C (1300°F) for 24hours in air.

Standard creep test specimens with rectangular cross-sections were electro-discharge machined from the heat treated bars and ground to remove the recast layer. Sheet specimens (gauge length ≈ 25.58mm and width ≈ 4.75mm) of two thicknesses (h), 0.51mm and 3.18mm were considered. Moreover, the sheet specimens were machined such that the orientation of the specimen width was within ±2 degrees of $< 100 >$, Fig. 1. Isothermal creep tests were carried out on these uncoated specimens in air under two conditions: (i) a test temperature of 760°C (1400°F) and a fixed nominal stress (force/initial area) of 758MPa (110ksi); and (ii) a test temperature of 982°C (1800°F) and a fixed nominal stress of 248MPa (36ksi).

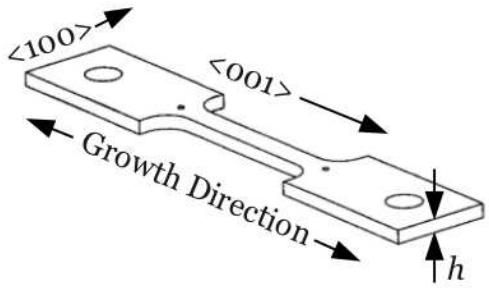

Figure 1: Schematic and orientation of the uncoated sheet specimen of PWA1484 single crystal superalloy used for creep test.

Metallographic studies were conducted on the fracture surface and near fracture surface of all the specimens using scanning electron microscopy (SEM). Specimens creep tested in air at 982°C developed surface oxides where as no oxidation was observed on the specimens creep tested at 760°C. The chemical analysis of the oxides formed due to environmental effects during the high temperature creep test (982°C) was performed using energy dispersive spectroscopy (EDS) in the SEM using an Apollo X silicon drift detector (SDD) at 20kV excitation voltage. The measured X-ray intensities were converted to atom% using an

atomic number absorbance and fluorescence (ZAF) program. To identify the oxides formed during high temperature creep exposure, X-ray diffraction (XRD) experiments were carried out in a Rigaku Ultima III diffractometer with a Cu Kα ($\lambda = 0.15406$nm) incident X-ray source. Electron backscatter diffraction known as orientation imaging microscopy (OIM) was carried out using a field emission gun (FEI Nova 230) scanning electron microscope (FEGSEM) in order to determine the local texture and microstructural changes, if any, due to recrystallization.

3. Results

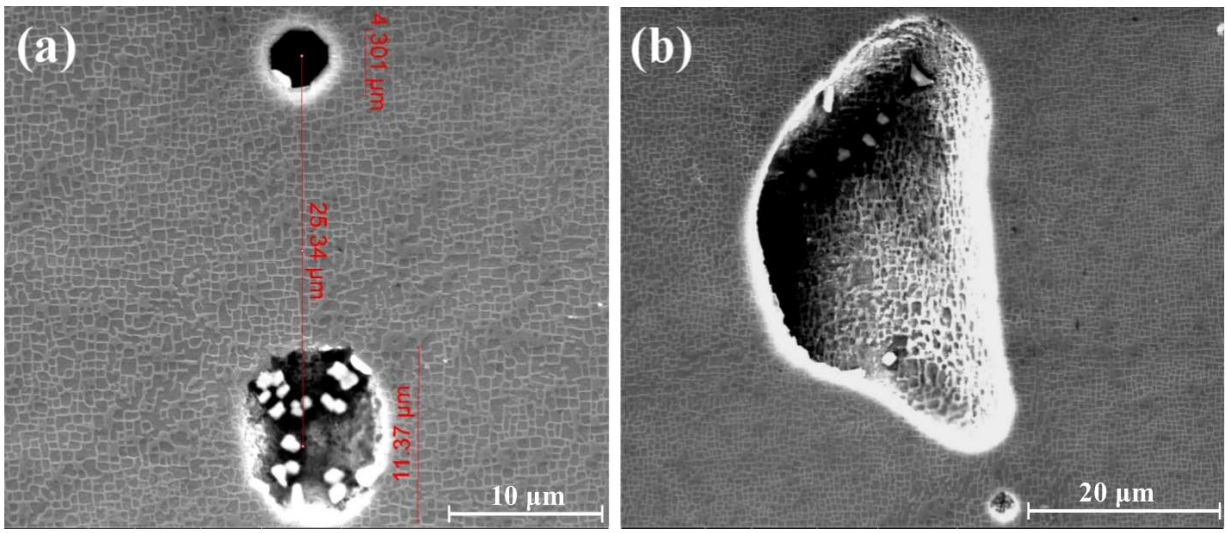

Figure 2: SEM images of the microstructure of PWA1484 single crystal superalloy showing initial porosity (a) Spherical homogenization pore and (b) Irregular shaped shrinkage pore.

The undeformed microstructure of the PWA1484 single crystal superalloy containing micropores is shown in Fig. 2. The microstructural characterization of the PWA1484 single crystal superalloy in the current work shows presence of micro pores formed during the solidification and homogenization processes as has been observed for other Ni-based single crystal superalloys (see e.g. [18, 19]). As shown in Fig. 2a the diameter of the spherical pores can be over $10\mu m$ and the irregular shaped pores can be even bigger as in Fig. 2b where the major diameter of the irregular pore is $45\mu m$. The spherical pores are generally formed during the homogenization processes and the irregular shaped pores are mainly formed during the solidification processes. The volume fraction of the micro voids is generally low but the voids are mostly confined to the interdendritic regions of the crystal which will result in a relatively high local void volume fraction.

The creep test specimens were machined from the bulk single crystal castings to eliminate the influence of variations in secondary dendrite arm spacing, micro-segregation patterns and initial porosity on the creep properties as in [10]. All creep tests were conducted at Metcut

Research Inc., Cincinnati, OH (USA). The elastic deformation was neglected and the creep data was recorded after applying the tensile load. The creep strain (ε_c) is defined as $\Delta l/l_0$, where l_0 is the initial gauge length. The creep data was recorded till a creep strain of 5% and after that the test was continued till rupture. Based on the results of Seetharaman and Cetel [10] creep tests of some specimens of thickness 3.18mm at 982°C/248MPa were interrupted after a test duration of 75hours ($\varepsilon_c = 0.63\%$) and 145.7hours ($\varepsilon_c = 5.5\%$). For the 0.51mm thick specimens few tests at 982°C/248MPa were interrupted after 51.2hours ($\varepsilon_c = 0.76\%$) to explore the evolution of damage as a function of the accumulated creep strain. Subsequently, the creep tests conducted at 760°C/758MPa will be termed the low temperature high stress creep tests and the tests at 982°C/248MPa will be termed the high temperature low stress creep tests.

3.1. Low temperature high stress results

3.1.1. Evolution of the creep strain

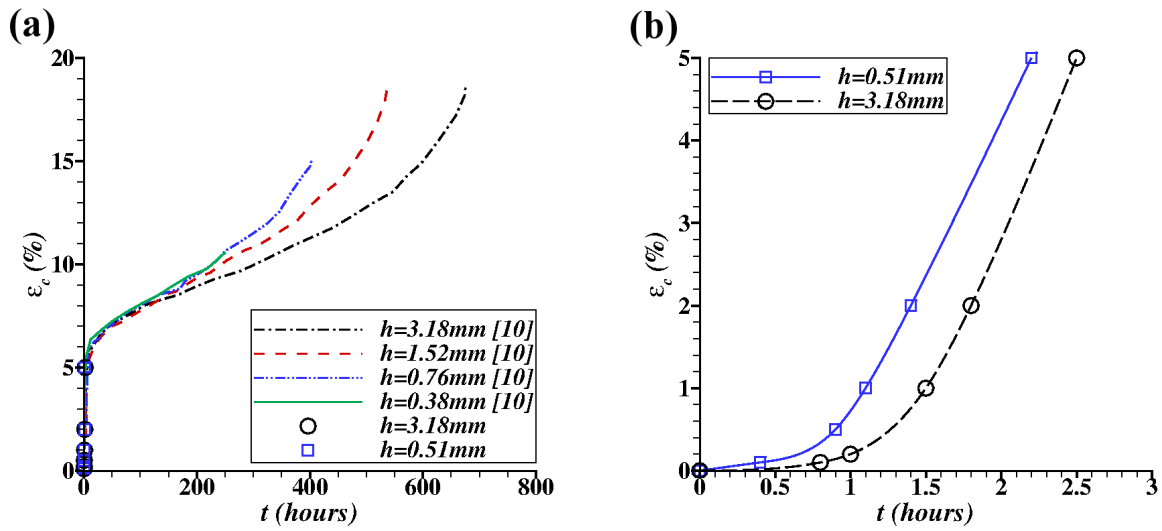

Figure 3: Creep strain (ε_c) vs. time (t) curves of sheet specimens of various thicknesses (h) creep tested at 760°C test temperature and 758MPa applied nominal stress. (a) Data from Seetharaman and Cetel [10] and the current work are compared. (b) Amplified Creep strain (ε_c) vs. time (t) curves for thicknesses h=0.51mm and 3.18mm.

The creep strain (ε_c) versus time (t) curves for the low temperature high stress loading condition for specimen thicknesses of 0.38mm, 0.76mm, 1.52mm and 3.18mm from the work of Seetharaman and Cetel [10] along with the results for specimen thicknesses of 0.51mm and 3.18mm from the current work are shown in Fig. 3a. Irrespective of the specimen thickness the primary creep regime extends to approximately 6% strain. The creep curves upto 5% strain for h=0.51mm and 3.18mm are shown in Fig. 3b. Both the specimens showed a brief incubation period followed by a constant primary creep rate. Under similar creep loading conditions Wilson and Fuchs [20] also reported incubation period in PWA1484 single crystal

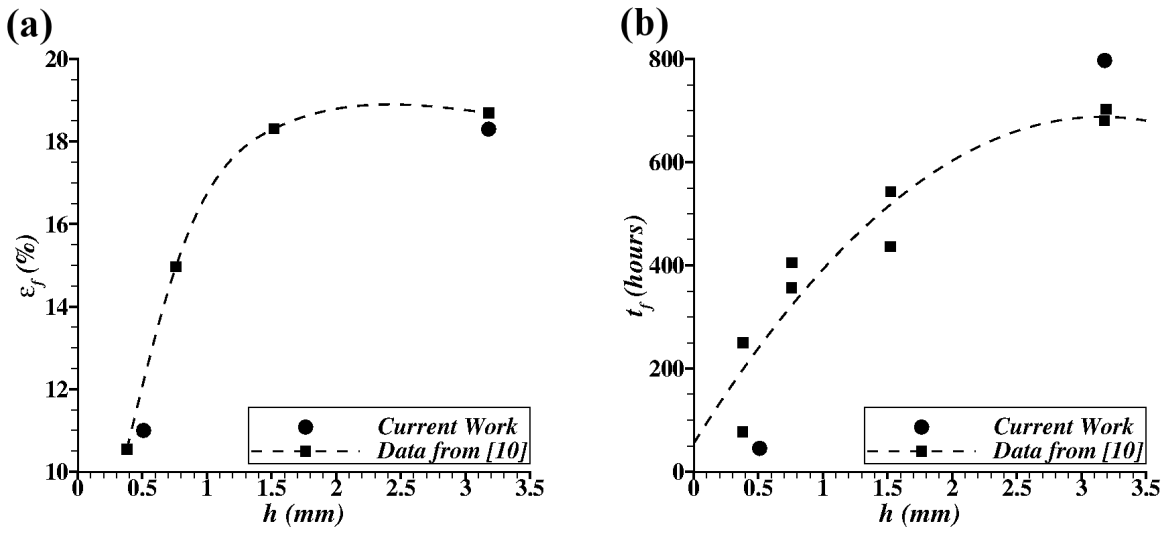

Figure 4: Effect of specimen thickness (h) on (a) creep strain to fracture (ε_f) and (b) time to fracture (t_f) of sheet specimens creep tested at 760°C test temperature and 758MPa applied nominal stress. Data from Seetharaman and Cetel [10] and the current work are compared.

superalloy. The difference in incubation period for specimen thicknesses 3.18mm and 0.51mm can be statistical in nature and not thickness dependent. Specimens of thickness 0.51mm reached 5% creep strain in 2.2hours and that of thickness 3.18mm reached in 2.5hours. The difference in time to 5% creep strain is very small as compared to the difference in final creep rupture time. As shown in Fig. 3a decreasing the specimen thickness from 3.18mm to 1.52mm resulted in a slight increase in steady state creep rate and showed an early inflection of the straight portion of the creep strain versus time curve. For specimens of thicknesses 0.76mm, 1.52mm and 3.18mm a deviation from the steady state creep towards tertiary creep is observed whereas no signature of tertiary creep is observed for specimens of thickness 0.38mm.

Creep damage initiates during primary creep, propagates during secondary or steady-state creep, and becomes unstable, resulting in failure, during tertiary creep. For the creep behavior shown in Fig. 3a, the creep rupture properties can be represented by creep strain to rupture i.e. creep ductility as shown in Fig. 4a. The creep strain to rupture for specimen of thickness 0.38mm is significantly lower than the specimen of thickness 3.18mm where pronounced tertiary creep is observed. The vanishing tertiary creep in thinner specimens shows the transition from creep-ductile to creep-brittle behavior with decreasing specimen thickness. As shown in Fig. 4a strain to final rupture remains nearly the same for specimen thickness 3.18mm and 1.52mm and with further decrease in thickness the creep ductility starts decreasing. Over 40% reduction in creep ductility is observed when specimen thickness is reduced from 3.18mm to 0.38mm. The reduction in creep life with decreasing specimen thickness is shown in Fig. 4b. The creep rupture life decreases monotonically with decreasing specimen thickness. An average reduction of about 60% in the creep rupture life is observed

when the specimen thickness is reduced from 3.18mm to 0.38mm.

3.1.2. Fractography

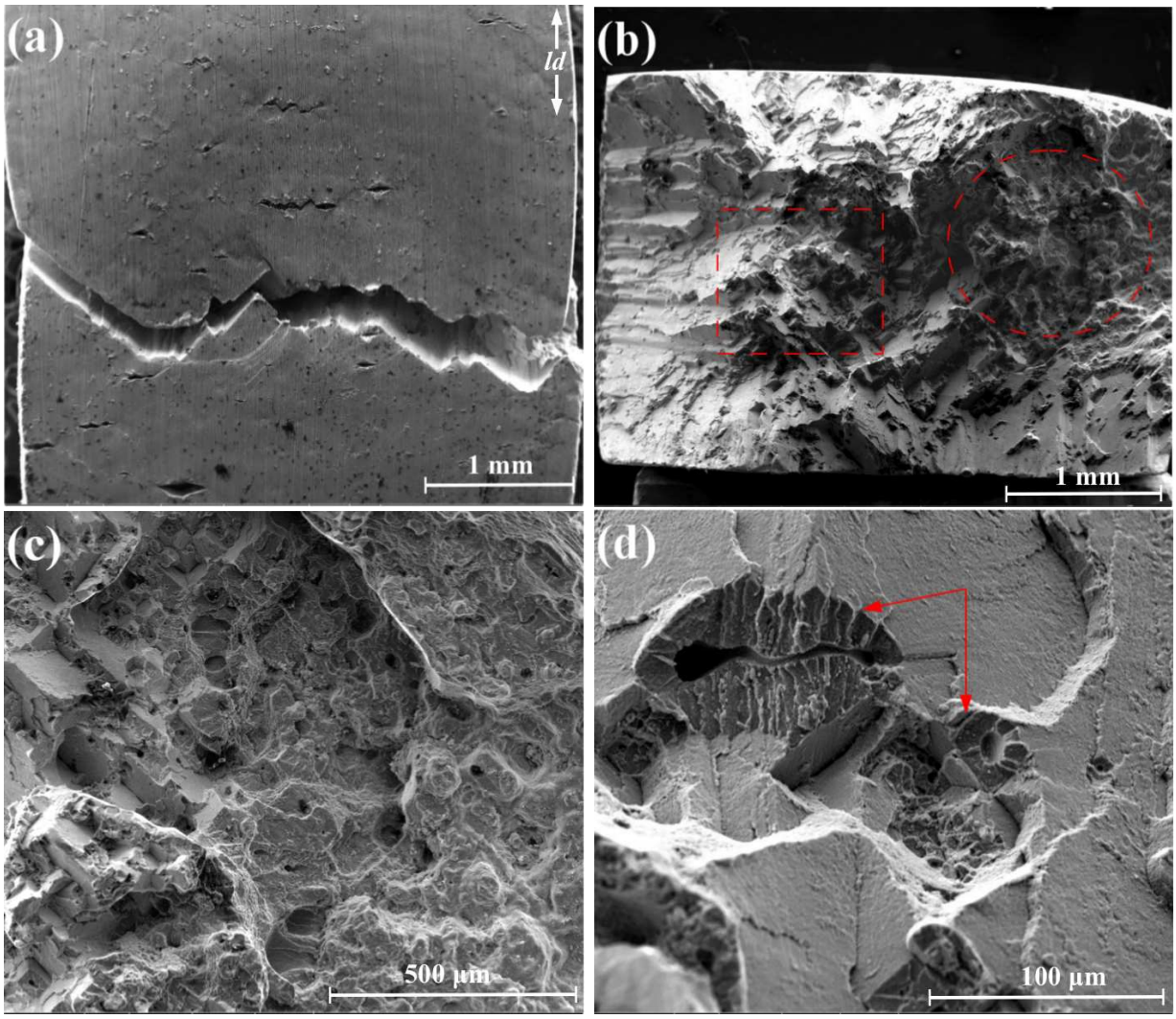

Figure 5: SEM images of the sheet specimen of thickness 3.18mm creep tested at 760°C/758MPa, (a) Specimen reconstructed after rupture (Loading direction is *ld* and thickness is into the plane); (b) Fracture morphology of upper half of the specimen in (a) (Loading direction is parallel to the Viewing direction); (c) Zoomed in view of the region enclosed with dotted circle in (b); (d) Zoomed in view of the region enclosed with dotted rectangle in (b).

To further explore the mechanism behind thickness debit effect, we performed standard fractography using secondary electron imaging (SE) in a scanning electron microscope (SEM). No surface oxidation was observed at this temperature. The reconstructed creep ruptured specimen of thickness 3.18mm is shown in Fig. 5a. The constant nominal stress creep loading direction in Fig.5a is marked as *ld*. The thickness of the sheet specimen is

into the plane of the image. It can be seen in Fig. 5a that the failure took place by very ductile failure mode. As visible in Fig. 5a, the failure of the specimen was accompanied by slight necking. The cross-sectional area near fracture surface is approximately 10% less than the cross-sectional area of the far gauge section. The signature of damage such as micro-cracks are also present away from the fracture region on the gauge section. The fracture surface inclined to the tensile axis can be seen in the reconstructed specimen. The fracture morphology in Fig. 5b shows the stepped cleavage planes and microvoiding. The crystallographic cleavage planes with traces of slip bands shows creep deformation by slip process. The cleavage then took place on the planes subjected to maximum resolved shear stress which are {111} family of planes as per Schmid factor. The edges of the projected fracture surface are inclined at an angle $\approx 45^\circ$ with respect to the loading axis i.e. $< 001 >$ crystallographic direction in Fig. 5a. This shows that the edges are along $< 011 >$ direction. It is important to note that {111} planes intersects with {100} planes along $< 011 >$ direction. The presence of numerous crystallographic facets indicate planar inhomogeneous plastic deformation. The zoomed in view of the region with void activity in Fig. 5c shows numerous shallow pores joined by shear along slip bands. In the other zoomed in view of the fracture surface in Fig. 5d interlinking of voids through crack formation is also observed. At several locations the fracture surface surrounding the voids are orthogonal to the loading axis as in brittle fracture (marked by arrow in Fig. 5d). Also we can observe two intersecting {111} crystallographic cleavage planes.

The reconstructed creep ruptured specimen of thickness 0.51mm is shown in Fig. 6a. Tensile creep loading loading direction in Fig.6a is marked as *ld* and the thickness is into the plane of the image. No necking was observed in the failed specimen of thickness 0.51mm and also there is no signature of damage present away from the fracture region on the gauge section. The orthogonal view of the region marked as dotted circle in Fig. 6a is shown in Fig. 6b. In the upper half of Fig. 6b we notice a region of uneven ductile fracture. This region contains numerous micro-cracks seemed to originate from micro-voids. A shear-lip inclined approximately at an angle of 45° to the loading axis can also be seen at the bottom of the image. The shear-lip contains numerous cleavage steps. At the root of the shear lip we can see the presence of river pattern [21]. The fracture morphology of the region marked with dotted rectangle in Fig. 6a is shown in Fig. 6c. This part of the fracture surface is moreover flat with right side edge inclined at an angle $\approx 45^\circ$ to the loading axis i.e. along $< 011 >$ crystallographic direction, as can be seen in the inset of the Fig. 6c. This implies that a major portion of the specimen is sheared along single plane through the thickness. Micro-cracks and voids are present on this surface as well. Figure 6d shows the zoomed in view of the fracture surface in between dotted circle and dotted rectangle in Fig. 6a. Here the presence of different intersecting crystallographic cleavage planes shows that the final rupture in this region occurred along more than one {111} family of planes.

The SEM image of the section above the fracture surface and normal to the loading direction of the specimen of thickness 0.51mm shown in Fig. 7 shows the presence of damage such as micro-cracks. The internal crack shown in Fig. 7a probably depicts the inter-linkage of big shrinkage pores and small homogenization porosities. Since the porosity distribution in the material is not uniform which means the isolated voids will not lead to void coalescence

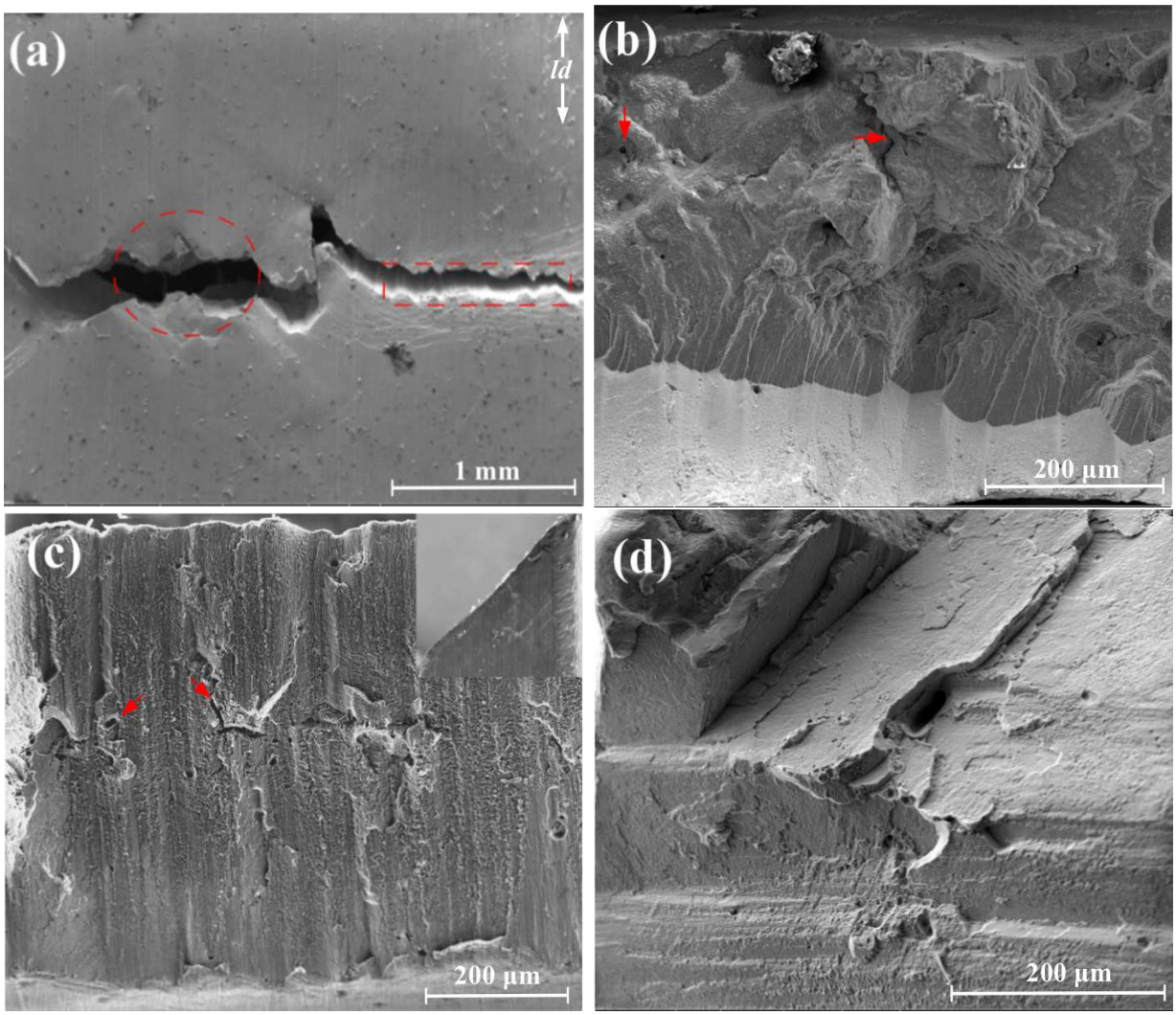

Figure 6: SEM images of the sheet specimen of thickness 0.51mm creep tested at 760°C/758MPa, (a) Specimen reconstructed after rupture (Loading direction is *ld* and thickness is into the plane); (b) Fracture morphology of the region marked with dotted circle in (a) (Loading direction is parallel to the Viewing direction); (c) Fracture morphology of the region marked with dotted rectangle in (a), the inset shows the right side view; (d) Zoomed in view of the fracture surface showing stepped cleavage planes.

but can initiate cracks as shown in Fig. 7b. Such internal crack like damages shown in Fig. 7a and b are also present in the specimen of thickness 3.18mm at the locations just above the fracture surface. Once the crack initiate from a void it propagates along the crystallographic planes with high resolved shear stresses. The presence of beads like structure at the far end of the crack in Fig. 7b shows inter-linkage of porosities though these micro-cracks.

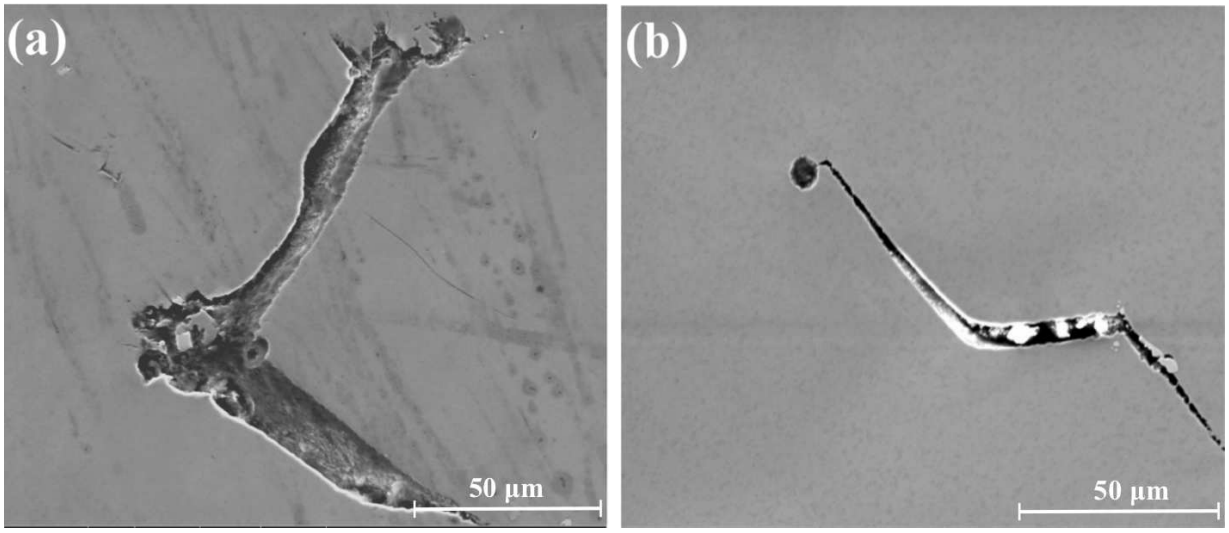

Figure 7: SEM image of a section normal to the loading direction of the specimen of thickness 0.51mm creep tested at 760°C/758MPa showing presence of micro-cracks above the fracture surface.

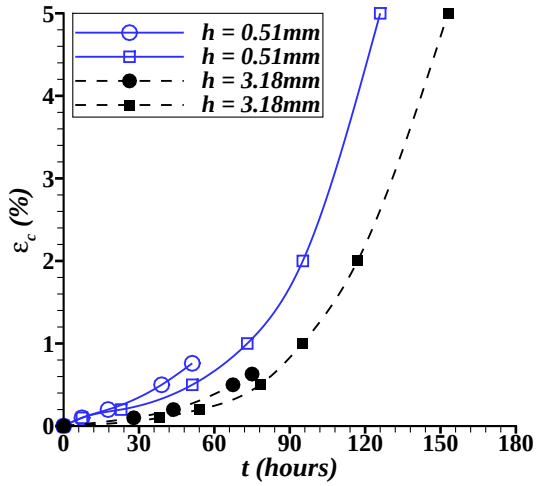

Figure 8: Creep strain (ε_c) vs. time (t) curves of sheet specimens of thicknesses (h) 0.51mm and 3.18mm creep tested at 982°C test temperature and 248MPa applied nominal stress till ε_c=5%. Creep tests interrupted after t=51.2hours for specimen thickness h=0.51mm and t=75hours for specimen thickness h=3.18mm are also shown.

3.2. High temperature low stress results

3.2.1. Evolution of the creep strain

Curves of creep strain versus time for specimen thicknesses of 0.51mm and 3.18mm tested at a temperature of 982°C and a nominal stress of 248MPa are shown in Fig. 8. The

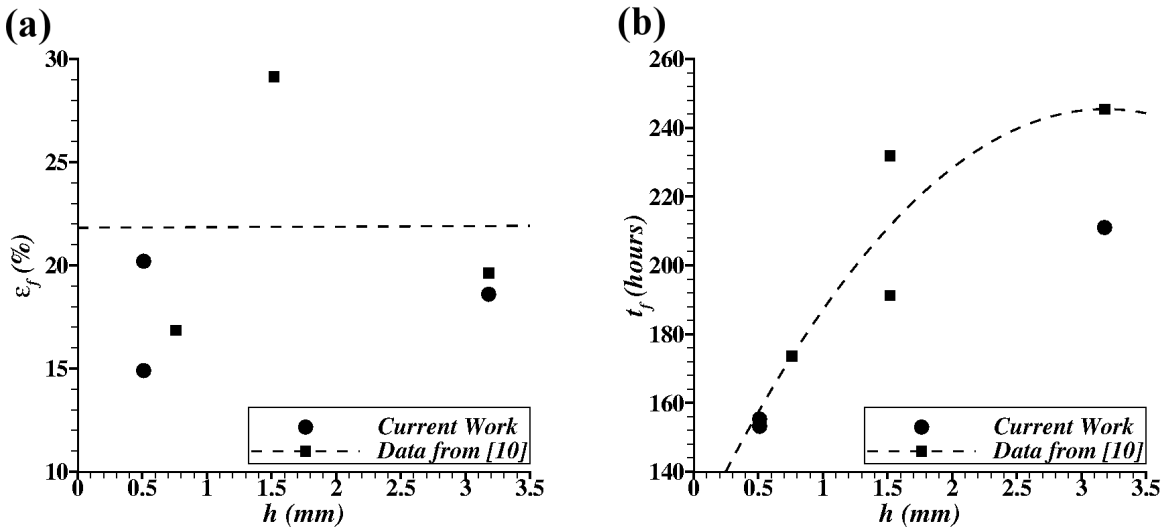

Figure 9: Effect of specimen thickness (h) on (a) creep strain to fracture (ε_f) and (b) time to fracture (t_f) of sheet specimens creep tested at 982°C test temperature and 248MPa applied nominal stress. Data from Seetharaman and Cetel [10] and the current work are compared.

creep strain versus time curves were recorded untill a creep strain of 5%. A few tests were continued to rupture while others were stopped at specified times in order to explore the evolution of damage as a function of accumulated creep strain. The negligible primary creep and absence of well defined steady state creep are the major differences observed at high temperature low stress when compared with low temperature high stress creep. The shape of the creep curve shown in Fig. 8 can be well defined as inverted transient (primary) creep curve. As shown in Fig. 8 time to reach 5% creep strain for specimen of thickness 3.18mm is 152hours and for specimen of thickness 0.51mm is 125hours. The thickness debit effect at high temperature low stress test condition can be interpreted as increased creep rate with decreasing thickness even at low strain levels. The creep curve of the interrupted tests in Fig. 8 confirms that the differences are indeed due to specimen thickness.

The creep strain to rupture and time to rupture for specimens of thickness 0.51mm and 3.18mm from the current work and for specimens of thickness 0.76mm, 1.52mm and 3.18mm from the work of Seetharaman and Cetel [10] are shown in Fig. 9a and b respectively. Unlike the case of low temperature high stress creep, no pattern in the overall creep ductility with decreasing specimen thickness is observed. The only major consequence of thickness debit effect as shown in Fig. 8 and in [10] is the increased creep rate with decreasing thickness. This increased creep rate does lead to decrease in rupture life with decreasing thickness as shown in Fig. 9b. Specimen of thickness 3.18mm fractured after a test duration of 210hours whereas specimens of thickness 0.51mm fractured after 155hours leading to a reduction of about 25% in creep rupture life.

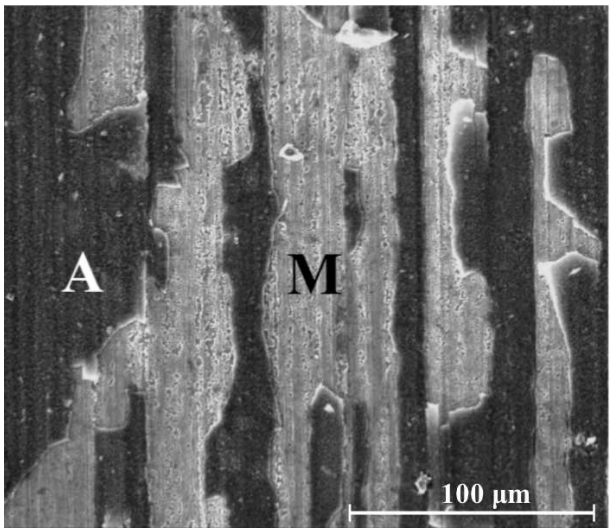

Figure 10: SEM image of the shoulder region (unstressed) of the creep tested specimen. A→Al-rich oxide and M→Mixed oxide.

3.2.2. Metallographic and Chemical Analysis

The excellent oxidation resistance of PWA1484 single crystal superalloy has been shown by Cetel and Duhl [17]. But the formation of multi-layer oxide film on the surface of uncoated test specimens creep tested in air at high temperature is unavoidable. Unlike the creep tests at 760°C significant surface oxidation was observed during the creep tests at 982°C. We analyzed the surface of the creep tested samples in a SEM using secondary electron (SE) imaging. Figure 10 shows the shoulder region of the grip of the creep tested specimen where no creep deformation is present. The image clearly shows the presence of two different layers. The brighter being the top layer and the darker being the bottom layer, suggesting the spallation of the brighter layer. The spallation of oxide layers at metal/alumina interface in PWA1484 superalloy has been discussed by Mennicke et al. [22] and Nychka et al. [23]. The grip region of all specimens tested at 982°C/248MPa show similar surfaces.

In contrast to the near grip region of the creep tested specimen, the gauge region of different specimens have different textures depending on the creep exposure time. Figure 11 and 12 shows different texture of the gauge region surface oxide after different creep exposure times for the specimen of thickness 3.18mm and 0.51mm respectively. After 75hours of creep exposure time for specimen of thickness 3.18mm and 51.2hours of creep exposure time for specimen of thickness 0.51mm the gauge surface shows a single oxide layer marked as layer-A in Fig. 11a and 12a. With the continuing creep exposure after 145.7hours as in Fig. 11b the oxide layer-A on the specimen gauge surface develops cracks perpendicular to the loading direction. These cracks expose metal to the air for further oxidation. The oxides formed in the open cracks are shown in Fig. 11c and 12b for the specimens of thickness 3.18mm and 0.51mm. This shows that the surface crack in layer-A were arrested due to further oxidation.

An extensive metallographic examination of a polished sample taken from the near frac-

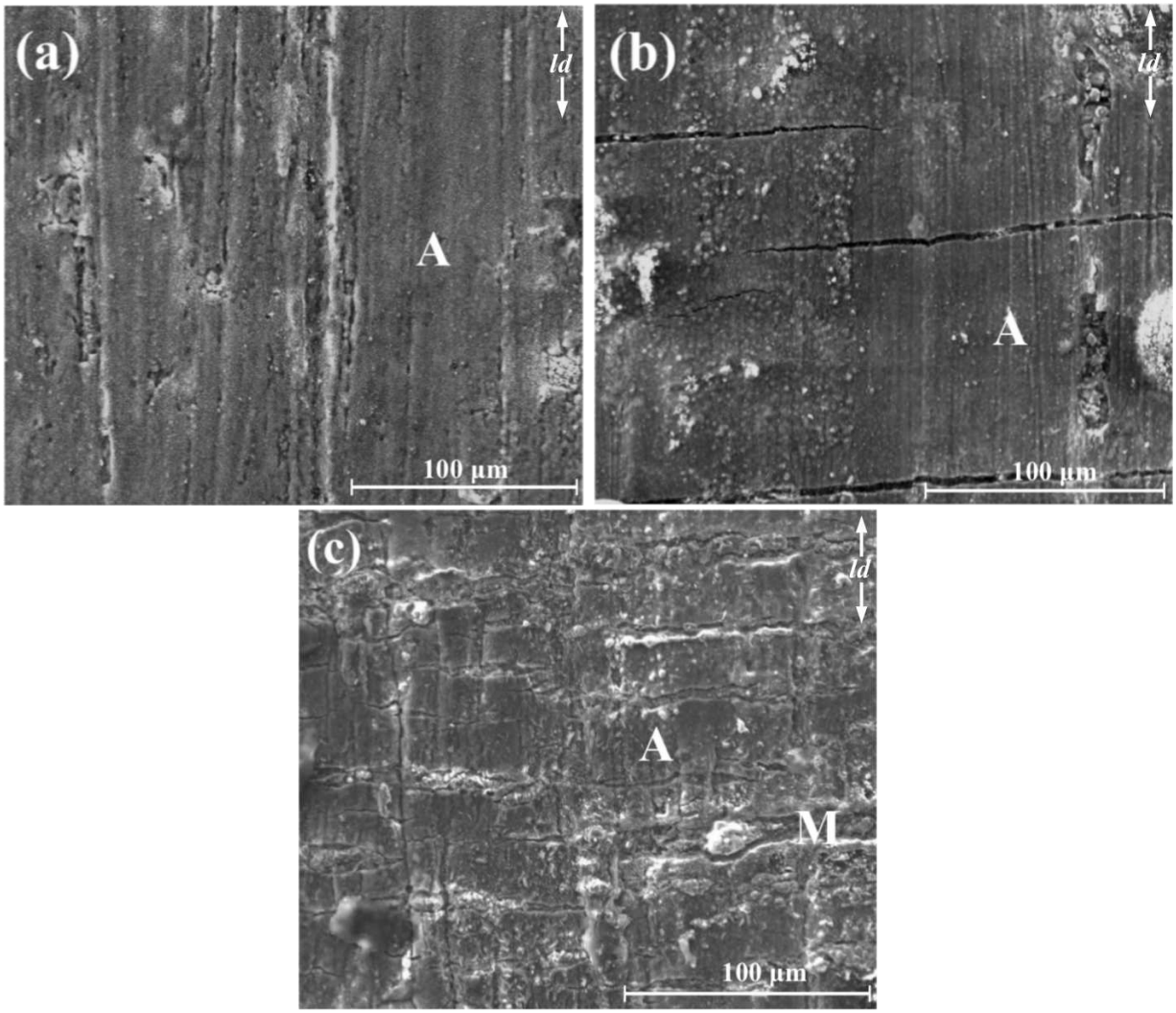

Figure 11: SEM image of the gauge region of the creep tested specimen of thickness 3.18mm (a) Test interrupted after 75hours, (b) Test interrupted after 145.7hours and (c) Gauge region above the fracture surface from the creep ruptured specimen (Loading direction is *ld*). A→Al-rich oxide and M→Mixed oxide.

ture region of the gauge section of the creep ruptured specimens showed the presence of different layers of oxides and microstructure of the alloy. One of the image taken from the near fracture zone of the creep ruptured specimen is shown in Fig. 13. Here we can clearly notice three layers of oxides (layer-N, M and A) and subsequent layers of the microstructure (L1, L2 and the rafted $\gamma^{'}$). The very first layer just after the oxide layer-A is marked as layer-L1 and as shown in the Fig. 13 no $\gamma^{'}$ precipitates are present in this layer. Two interesting features observed in layer-L1 ($\gamma^{'}$-free layer) are the presence of big voids and faceted precipitates (marked with an arrow). The layer-L2 after $\gamma^{'}$-free layer is the depleted $\gamma^{'}$ precipitate layer. The extensive rafting of $\gamma^{'}$ normal to the loading direction in the bulk of the material is consistent with other observations on superalloys characterized by small

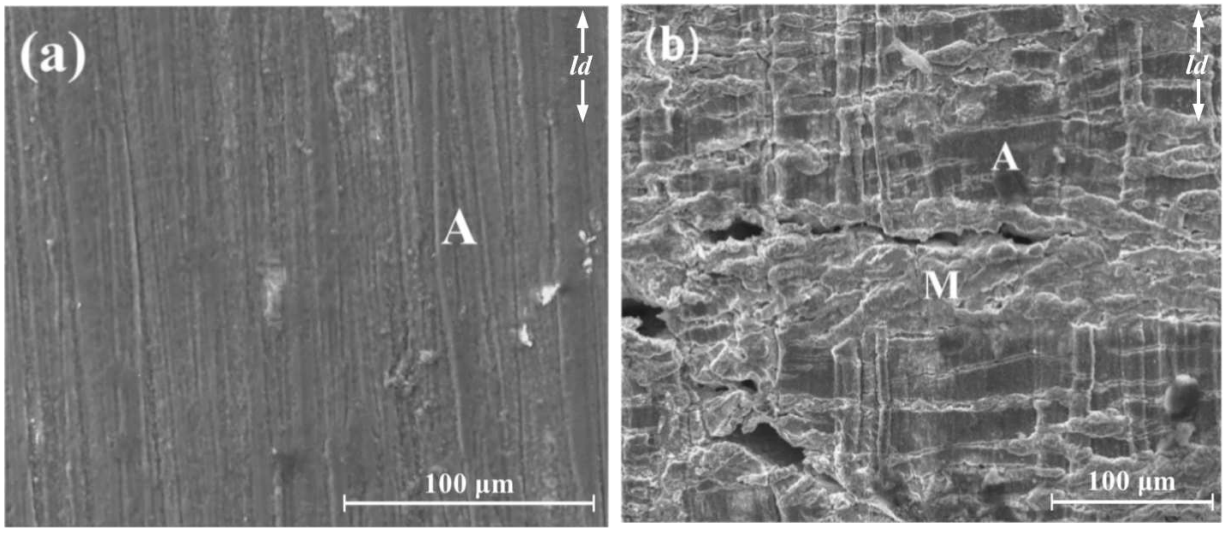

Figure 12: SEM image of the gauge region of the creep tested specimen of thickness 0.51mm (a) Test interrupted after 51.2hours and (b) Gauge region above the fracture surface from creep ruptured specimen (Loading direction is *ld*).A→Al-rich oxide and M→Mixed oxide.

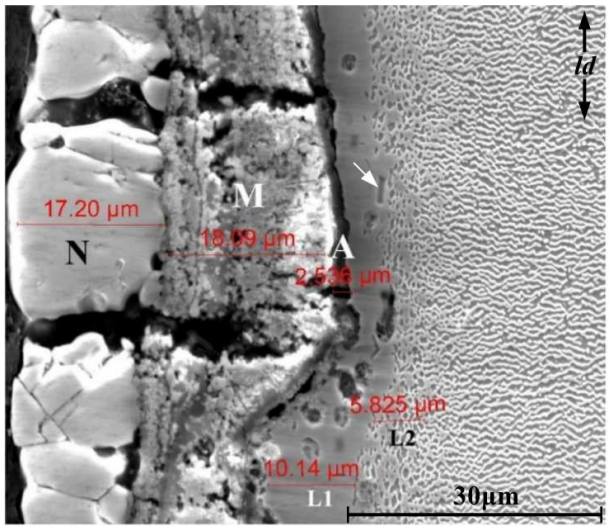

Figure 13: SEM image showing three layers of oxides (N→Ni-rich, M→mixed and A→Al-rich oxides) and subsequent layers of the microstructure (L1→ γ'-free, L2→ γ'-reduced and rafted in the bulk). Arrow marks the presence of faceted precipitates in the L1 layer. Loading direction is *ld*.

negative misfit between the lattices of γ and γ' phases.

The first two oxide layers shown in Fig. 13 is present in small patches on the specimen surface both at stressed gauge section or unstressed grip section. The EDX spectra in Fig. 14 identifies layer-N as a Ni rich oxide layer. Extensive spallation of Ni rich oxide layer is also reported in [23]. Layer-M as per the EDX spectra is a mixed oxide of Ni, Al, Ta, Cr and Co.

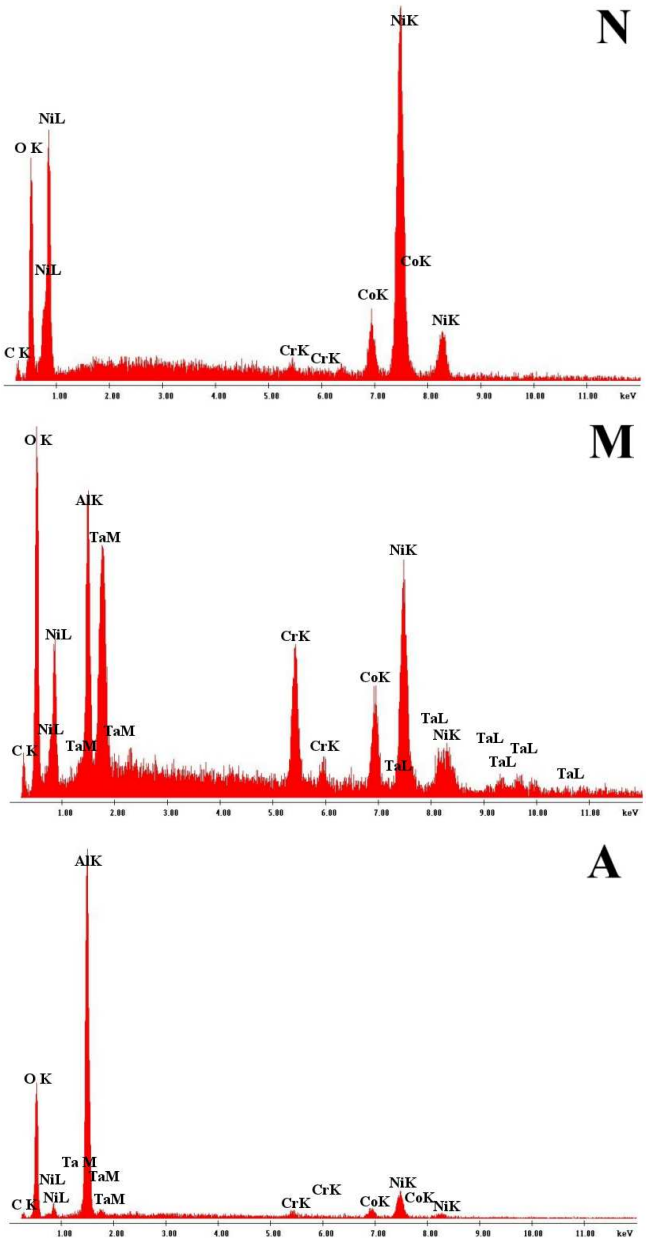

Figure 14: EDX spectra from the representative areas corresponding to N, M and A.

This mixed oxide layer precedes the Ni rich oxide layer and is also present in the cracks in adherent layer-A as shown in Fig. 11c and 12b. The adherent layer-A is the Al rich oxide as per EDX spectra in Fig. 14. The quantification of EDX spectra from the faceted precipitates in the γ'-free layer in Fig. 13 suggests the presence of an Al rich precipitate with the ratio of atom% of Ni and Al approximately equal to 1. Similar Al rich precipitates are reported in the oxidation studies of CMSX-10 by Akhtar et al. [24].

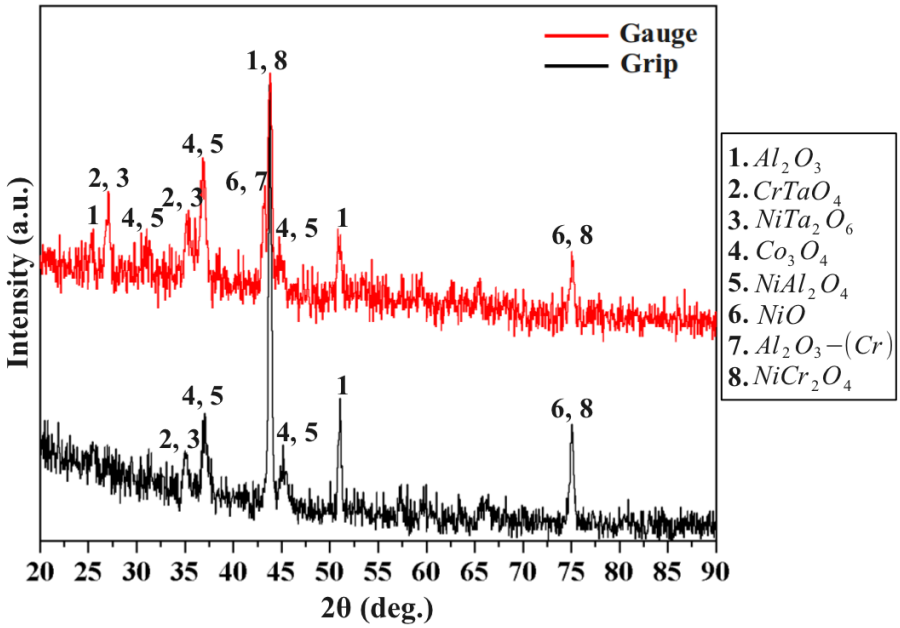

Figure 15: XRD patterns from the shoulder region of the grip section (unstressed) and from the near fracture region of the gauge section of the specimen creep tested at 982°C/248MPa. Intensities (in arbitrary units) are vertically offset to show the data effectively.

The oxide phase identification as determined from XRD patterns in Fig. 15 reveal the formation of different oxides and spinels namely Cr doped Al_2O_3, Al_2O_3, Co_3O_4, NiO, $NiTa_2O_6$, $CrTaO_4$, $NiAl_2O_4$ and $NiCr_2O_4$. Several diffraction peaks from these different oxides overlap and are shown in Fig. 15 for the sake of completeness. Combining Fig. 13, 14 and 15 we can comment on the sequence of phase transformation occurring due to oxidation. The formation of the first external layer i.e. mainly NiO leads to nickel depletion in the near surface region resulting in increased aluminum concentration in this region. This shift in composition in the near surface region leads to the formation of Al-rich precipitates. With continued exposure to air at high temperature further oxidation takes place till a stable alumina layer is formed on the cost of γ' and other Al-rich precipitates formed due to compositional shift. The environmental degradation of the uncoated specimens creep tested at 982°C/248MPa is independent of the specimen thickness.

Another observation made from the EBSD inverse pole figures, Fig. 16, of the γ' precipitate free zone in Fig. 13 is the presence of recrystallized grains. Figure 16 represents an area of $9.1 \times 4.6\mu m^2$. The electron beam was scanned in steps of $0.1\mu m$ and the EBSD pattern was indexed using the nickel fcc phase. Dynamic recrystallization in the precipitate free zone under the oxide scale occurred during the creep test at 982°C/248MPa and in both the specimens of thickness 3.18mm and 0.51mm. The dynamic recrystallization mainly resulted in sub grain boundaries and recrystallization twin boundaries. The grain boundaries formed during recrystallization may lead to creep cavitation. An increase in voids in the precipitate free zone can be seen in the Fig. 13. Hence the oxidation does not only contribute to

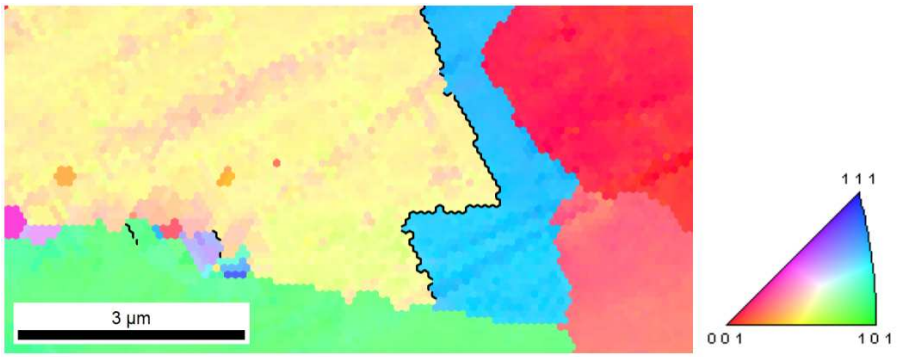

Figure 16: Inverse pole figure map of the $\gamma^{'}$-free zone in the specimen creep tested at 982°C/248MPa. The map is given in [001] orientation. The grain orientations can be seen from the color-coded stereographic triangle. Σ_3 (twin) boundaries are marked in black.

reduction in load carrying cross-sectional area but also produces a boundary layer which is more prone to damage. The size of the recrystallized zone formed due to oxidation during high temperature creep will be independent of the specimen thickness and will affect thin specimen more than the thicker ones.

The evolution of damage in the form of micropores and micro-cracks with the high temperature creep deformation for specimen thicknesses 0.51mm and 3.18mm is shown in Fig. 17. Figure 17a and b compares the accumulated damage in the gauge region of the specimen interrupted after 51.2hours (ε_c=0.76%) and in the region above fracture surface of the creep ruptured (ε_f=14.9% and t_f = 155hours) specimen of thickness 0.51mm. The comparison reveals an increase in porosity with increasing creep deformation. Several pores are elongated in the loading direction and also many pores have developed micro-cracks perpendicular to the loading direction. Similarly Figure 17c and d compares the accumulated damage in the gauge region of the specimen interrupted after 75hours (ε_c=0.63%) and in the region above fracture surface of the creep ruptured (ε_f=18.6% and t_f = 210hours) specimen of thickness 3.18mm. Here also we can draw similar conclusions. The increased number of pores observed after creep deformation suggests growth of existing pores and nucleation of new pores. Epishin and Link [25] observed similar growth of initial pores in the interdendritic regions and nucleation of new pores at the γ-$\gamma^{'}$ interfaces. A comparison of Fig. 17b and d, shows more damage in the creep ruptured specimen of thickness 3.18mm as compared to the specimen of thickness 0.51mm. Link et al. [19] discussed that the deformation induced porosity increases with time and it is worth noting that the specimen of thickness 0.51mm ruptured after 155hours where as the specimen of thickness 3.18mm ruptured after 210hours.

3.2.3. Fractography

The SEM image of the reconstructed creep ruptured specimen of thickness 3.18mm is shown in Fig. 18a. Tensile creep loading direction is marked as *ld* and the thickness is into the plane of the image. No necking was observed in the failed specimen. The presence of micro-cracks perpendicular to the loading direction can be seen in the gauge section away

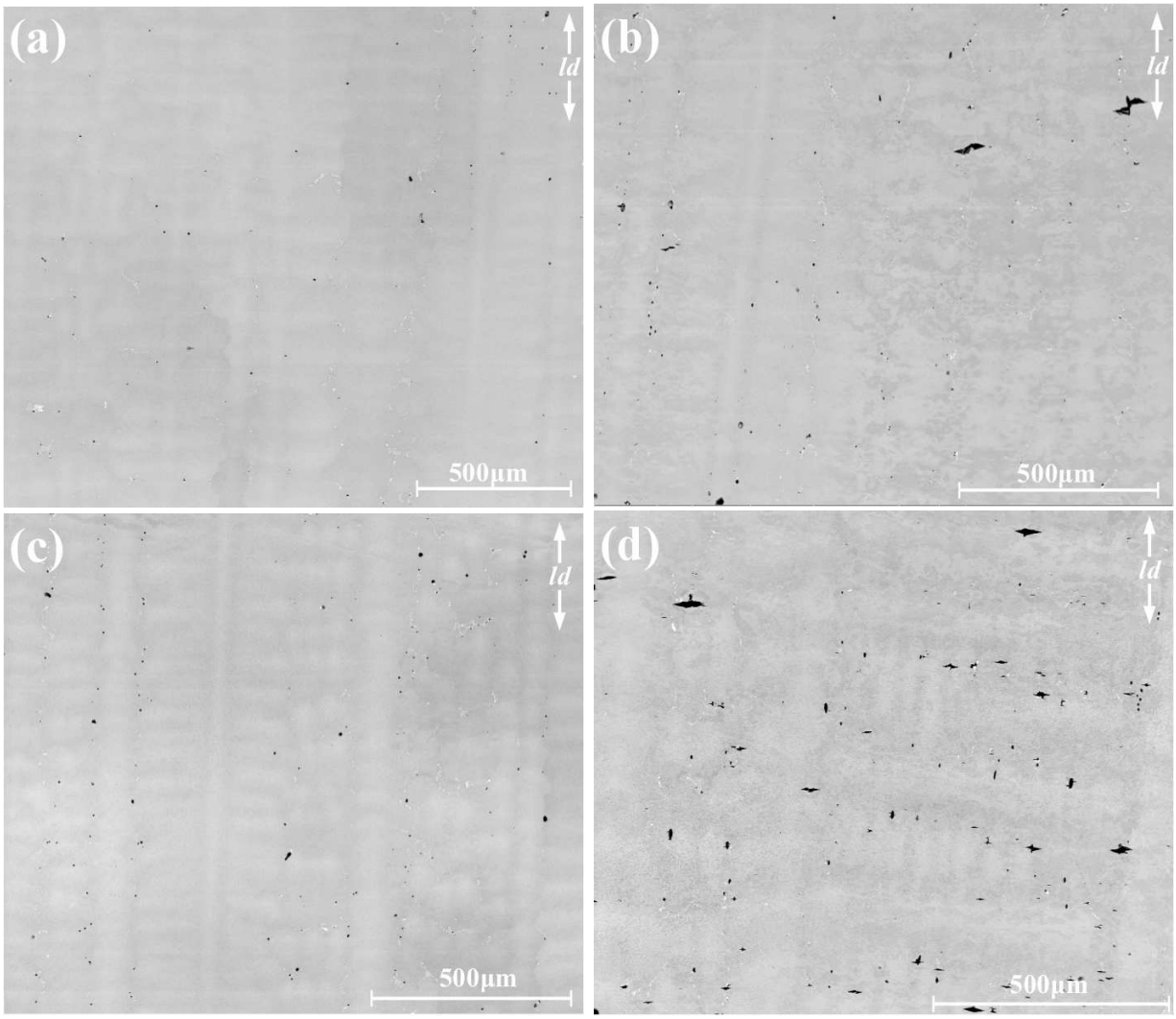

Figure 17: SEM image showing evolution of damage in the specimens creep tested at 982°C/248MPa. (a) specimen thickness h=0.51mm after 51.2hours, (b) specimen thickness h=0.51mm after rupture, (c) specimen thickness h=3.18mm after 75hours, and (d) specimen thickness h=3.18mm after rupture (Loading direction is ld).

from the fracture surface. A homogeneous fracture morphology suggesting dimple rupture can be seen in Fig. 18b. The zoomed in view of the fracture morphology in Fig. 18c shows the presence of micro-voids and micro-cracks in the cup-like depressions. This suggests that the rupture occurred due to nucleation, growth and coalescence of voids and not because of the cracks initiated in the oxide layer as these cracks were arrested due to further oxidation.

The reconstructed creep ruptured specimen of thickness 0.51mm is shown in Fig. 19a. Tensile creep loading direction is marked as ld and the thickness is into the plane of the image. Here also no necking was observed in the failed specimen. The presence of micro-cracks perpendicular to the loading direction in the gauge section away from the fracture

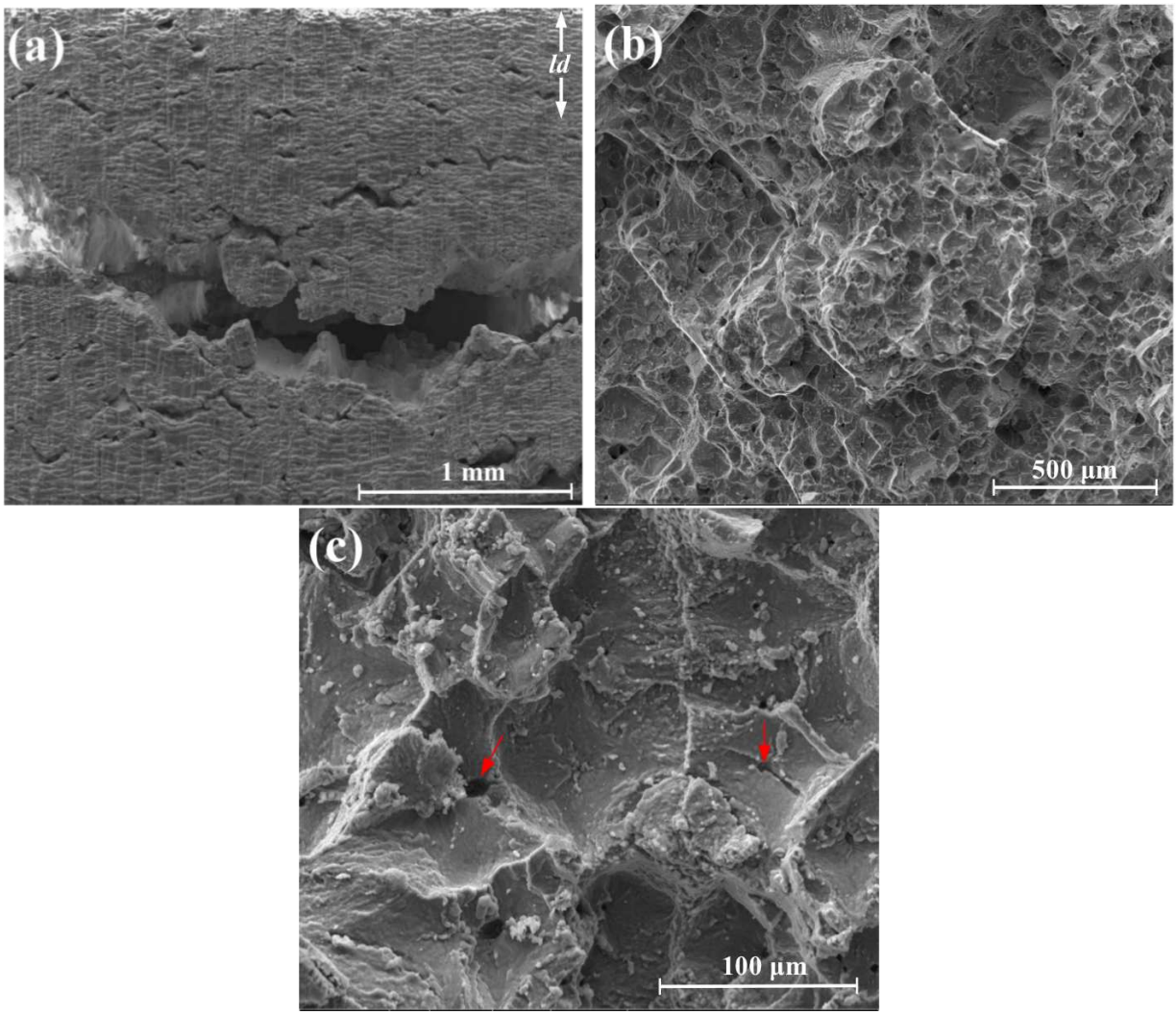

Figure 18: SEM images of the sheet specimen of thickness 3.18mm creep tested at 982°C/248MPa, (a) Specimen reconstructed after rupture (Loading direction is *ld* and thickness is into the plane); (b) Fracture morphology of the specimen in (a) (Loading direction is parallel to the Viewing direction); (c) Zoomed in view of the fracture morphology in (b).

surface as in the case of specimen of thickness 3.18mm can be seen. The fracture surface obtained with specimen thickness 0.51mm is not homogeneous as it contains both dimple rupture and cleavage steps. The region of the fracture surface in Fig. 19b shows the presence of voiding and irregular bulged areas. This type of fracture morphology is observed over a large fraction of the fracture surface. Moving across the width of the sample we can see the presence of cleavage steps at the ends. These cleavage steps are inclined to the loading direction as shown in Fig. 19c. The region surrounding the voids on the cleavage plane are orthogonal to the loading direction. This shows that the cracks perpendicular to the loading axis initiated from the voids and then continued on the crystallographic planes finally leading

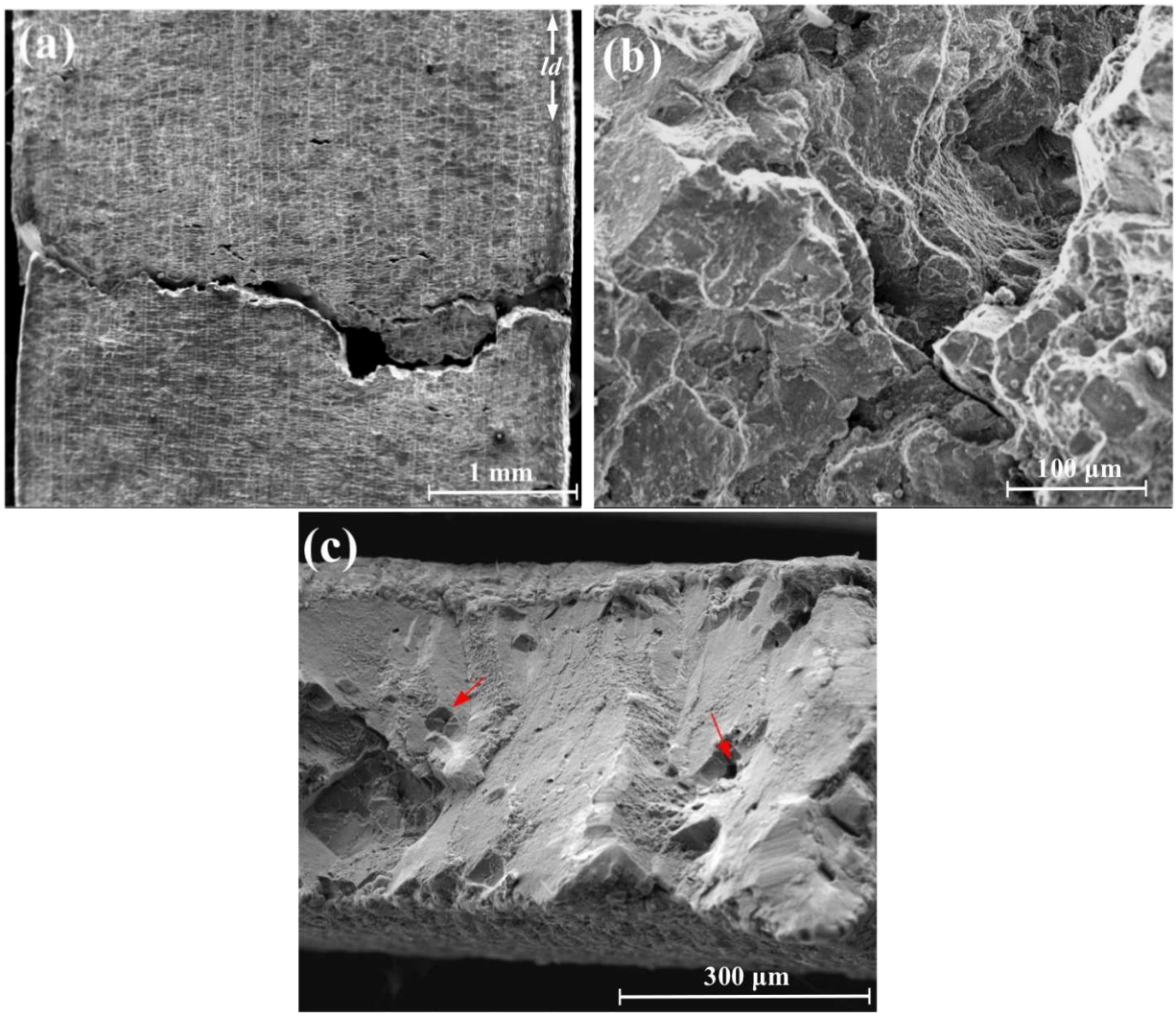

Figure 19: SEM images of the sheet specimen of thickness 0.51mm creep tested at 982°C/248MPa, (a) Specimen reconstructed after rupture (Loading direction is *ld* and thickness is into the plane); (b) Fracture morphology of the specimen in (a) showing ductile fracture (Loading direction is parallel to the Viewing direction); (c) Fracture morphology of the specimen in (a) showing cleavage steps (Loading direction is parallel to the Viewing direction).

to cleavage. The difference in the fracture morphology of specimens of thicknesses 0.51mm and 3.18mm can also be related to the evolution of damage as shown in Fig. 17.

4. Discussion

The thickness debit effect in the creep properties of sheet specimens of PWA1484 Ni-base single crystal superalloy at two creep test conditions are significantly different. At low temperature high stress creep (760°C/758MPa) thickness debit effect is observed mainly

in the form of significant reduction in creep ductility with decreasing specimen thickness which finally led to reduction in creep rupture life. The specimen of thickness 3.18mm showed pronounced tertiary creep and damage than the specimens of thickness 0.38mm. As per Ashby and Dayson [26] under constant load creep acceleration in the creep rate in the tertiary stage is caused by changes in external geometry and damage. The damage level increases with increasing tertiary creep strain. With decreasing thickness the sheet specimen becomes creep brittle and are not damage tolerant, so developing microcracks propagate rapidly to cause low ductility failure, terminating the creep curve with little or no tertiary stage.

In the microstructural characterization of the specimens creep ruptured at 760°C/758MPa the region perpendicular to the loading direction surrounding the voids shows that Mode-I crack initiated from the voids. These Mode-I cracks interlinked with the Mode-II cracks on the planes with maximum resolved shear stresses which are {111} crystallographic planes leading to final fracture. This is in line with the observations made by Sherry and Pilkington [27]. Based on finite element analysis of porosity evolution in an fcc single crystal under creep loading, Srivastava and Needleman [28] reported that at low stress triaxiality values damage in the form of void growth is limited. But showed that a very high stress concentration can develop in the vicinity of the void on the plane perpendicular to the loading direction. This will lead to immediate loss of stress carrying capacity and would be more pronounced for thinner specimens. This finding supports Baldan's [8] argument that the creep response is controlled by the crack size to section size ratio. At least for the cases where no environmental damage effects are observed as in the creep tests at low temperature high stress conditions.

Thickness debit effect at high temperature low stress creep (982°C/248MPa) is marked by increase in creep rate even at low creep strain levels and reduction in creep rupture life with decreasing thickness. No conclusive reduction in the creep ductility is observed in the creep tests here and in [10]. Hüttner et al. [12, 13] did observe loss of creep ductility and increased creep rate with decreasing thickness for both coated and uncoated specimens of René N5 single crystal superalloy at a test temperature of 1253K (980°C). Interestingly Hüttner et al. [12] reported that uncoated specimens were less influenced by thickness change as compared to coated specimens whereas Doner and Heckler [3, 5] observed no thickness debit in single crystal CMSX-3 mini-flat aluminide coated specimens tested in air and uncoated specimens tested in high purity argon.

The microstructural characterization of interrupted creep test and creep ruptured specimens at 982°C/248MPa confirmed spallation of oxides and formation of adherent Al rich oxide layer. The cracks formed on the oxide layer were arrested due to further oxidation. The surface oxidation led to the formation of γ'-precipitate free and depleted zone. These precipitate free zones under went dynamic recrystallization resulting in the formation of sub grains and recrystallized twins. The environmental degradation of the specimen is independent of the thickness and hence will affect the thinner specimens more than the thicker ones. The comparison of accumulated damage in the form of micropores and micro-cracks showed that the specimens of thickness 3.18mm accumulated more damage than the specimens of thickness 0.51mm. This can be related to the fracture morphology where a transition from

homogeneous dimple rupture in case of thick specimens to a mixed mode of voiding and cleavage type rupture in case of thin specimens was observed. No loss of creep ductility with decreasing specimen thickness suggests a strain controlled failure rather stress controlled. Under such cases the creep rupture will occur after a critical strain and the increase in the creep rate with decreasing specimen thickness will inherently lead to reduction in creep rupture life.

In the absence of environmental damage and void nucleation, initial pores are the most favored sites for crack nucleation under low temperature high stress test conditions. The thickness debit effect in PWA1484 Ni-base single crystal superalloys at 760°C and 758MPa can be explained by a void growth model for a single crystal and a criteria for crack nucleation from an isolated void as in [29]. At high temperature low stress, the observed thickness debit effect in the uncoated specimens tested in air can be partly explained in terms of continuous loss of load carrying cross section due to oxidation as in [16] and formation of a boundary damage layer due to dynamic recrystallization as in [14, 15]. Based on the current observations and the results obtained from the aluminide coated specimens by Hüttner et al. [12, 13], nucleation and growth of porosity and cracks together with surface oxidation and formation of boundary damage layer will completely explanation the observed thickness debit effect.

5. Summary and conclusion

Isothermal, constant nominal stress creep test at two test conditions 760°C/758MPa and 982°C/248MPa were performed on the uncoated sheet specimens of thickness 3.18mm and 0.15mm. To understand the contribution of different mechanisms leading to thickness debit effect, some of the creep tests at 982°C/248MPa were interrupted after predefined time. The observed thickness debit at two test conditions can be summarized as:

Low temperature high stress (760°C/758MPa):

1. At low temperature high stress decrease in specimen thickness from 3.18mm to 0.38mm resulted in over 40% reduction in creep strain to rupture and around 60% reduction in time to rupture. The thickness debit effect is not pronounced at low strain levels and can be due to the statistical nature of the incubation period observed at low temperature creep.

2. The deformation of the initial porosity and nucleation of cracks from the deformed pores leads to creep rupture at low temperature high stress. A reduction in damage tolerance with decreasing specimen thickness is mainly responsible for the observed thickness debit effect.

High temperature low stress (982°C/248MPa):

1. The thickness debit effect is moderate under high temperature low stress creep. A decrease in specimen thickness from 3.18mm to 0.51mm resulted in about 25% reduction in time to rupture. The thickness debit effect can be conclusively observed at

low strain. Time to reach 5% creep strain decreased by 18% with specimen thickness decreasing from 3.18mm to 0.51mm.

2. The high temperature creep test in air resulted in the formation of surface oxides. Spallation of certain oxide layers and formation of adherent Al-rich oxide was observed. The cracks formed in the adherent oxide layer exposed the metal and were arrested due to further oxidation.

3. The dynamic oxidation of the uncoated specimen under high temperature low stress creep resulted in the formation of a $\gamma^{'}$-precipitate free zone. The precipitate free zone underwent dynamic recrystallization resulting in the formation of sub grains. Increased porosity in this zone was observed.

4. A transition from homogeneous dimple fracture due to void nucleation, growth and coalescence to a mixed mode of voiding and cleavage was observed with decreasing specimen thickness. This again confirmed that the specimen became less damage tolerant with decreasing thickness.

Acknowledgments

We are grateful for the financial support provided by the Air Force Research Laboratory (AFRL/RXLM) to the University of North Texas under the Institute for Science and Engineering Simulation (ISES) Contract FA8650-08-C-5226.

References

[1] Gell M., Duhl D.N. and Giamei A.F. The development of single crystal superalloy turbine blades. Superalloys 1980, 205-214.

[2] Koff B.L. Gas turbine technology evolution: A designers perspective. Journal of Propulsion and Power, 2004, 20, 577595.

[3] Doner M. and Heckler J.A. Effects of section thickness and orientation on creep rupture properties of two advanced single crystal alloys. SAE technical paper 851785, (Society of Automative Engineers Inc.), 1985.

[4] Duhl D.N. Directionally solidified superalloys, in Superalloys II, C.T. Sims, N.S. Stoloff, and W.C. Hagel, (Eds.), (John Wiley, New York), 1987, 189-214.

[5] Doner M. and Heckler J.A. Identification of mechanism responsible for degradation in thin-wall stress rupture properties. Superalloys 1988, Proceedings of the 6^{th} international symposium on superalloys, The metallurgical society, Warrendale, PA, 1988, 653-662.

[6] Duhl D.N. Single crystal superalloys, Superalloys, Supercomposites and Superceramics, J.K. Tien and T. Caulfield (Eds.), Academic Press, Inc. New York, NY, 1989, 149-182.

[7] Pandey M.C. and Taplin D.M.R. Prediction of rupture lifetime in thin sections of a nickel base superalloy. Scripta Metallurgica et Materialia, 1994, 31(6), 719-722.

[8] Baldan A. On the thin-section size dependent creep strength of a single crystal nickel-base superalloy. Journal of materials science, 1995, 30, 6288-6298.

[9] Henderson P.J. Creep of single crystal Ni-base superalloy in thick and thin section forms. Creep and fracture of engineering materials and structures, ed. J.C. Earthman and F.A. Mohamed, 1997, 697-706.

[10] Seetharaman V. and Cetel A.D. Thickness Debit in Creep Properties of PWA1484. Superalloys 2004, TMS (The Minerals, Metals and Materials Society), 2004, 207-214.

[11] Henderson P.J. Creep of coated and uncoated thin-section CMSX-4. Materials for advanced power engineering, (Forschungszentrum Juelich GmbH), 1998, 1559-1568.

[12] Hüttner R., Völkl R., Gabel J. and Glatzel U. Creep behavior of thick and thin walled structures of a single crystal NI-base superalloy at high temperatures-Experimental method and results. Superalloys 2008, R.C. reed, K.A. Green, P. Carron, T.P. Gabb, M.G. Fahrmann, E.S. Huron and S.A. Woodard, TMS (the minerals and materials society), 2008, 719-723.

[13] Hüttner R., Gabel J., Glatzel U. and Völkl R. First creep results on thin-walled single-crystal superalloys. Material science and engineering A, 2009, 510-511, 307-311.

[14] Gullickson J., Needleman A., Staroselsky A. and Cassenti B. Boundary damage effects on the evolution of creep strain. Modelling and Simulation in Materials Science and Engineering, 2008, 16, 075009.

[15] Cassenti B. and Staroselsky A. The effect of thickness on the creep response of thin-wall single crystal components. Materials Science and Engineering A, 2009, 508(1-2), 183-189.

[16] Bensch M., Preußner J., Hüttner R., Obigodi G., Virtanen S., Gabel J. and Glatzel U. Modelling and analysis of the oxidation influence on creep behaviour of thin-walled strutures of the single-crystal nickel-base superalloy René N5 at 980°C. Acta Materialia, 2010, 58, 1607-1617.

[17] Cetel A.D. and Duhl D.N. Second Generation Nickel Base Single Crystal Superalloy. Superalloys 1988, Proceedings of the 6th International Symposium on Superalloys, The Metallurgical Society, Warrendale, PA, 1988, 235-244.

[18] Anton D.L. and Giamei A.F. Porosity distribution and growth during homogenization in single crystals of a nickel-base superalloy. Materials Science and Engineering, 1985, 76, 173-180.

[19] Link T., Zabler S., Epishin A., Haibel A., Bansal M. and Thibault X. Synchrotron tomography of porosity in single-crystal nickel-base superalloys. Materials Science and Engineering A, 2006, 425 (1-2), 47-54.

[20] Wilson B. and Fuchs G. Primary creep: secondary gamma prime and the rhenium effect. JOM Journal of the Minerals, Metals and Materials Society, 2008, 60 (7), 43-48.

[21] ASM Handbook, Fractography, Volume 12, 1987.
[22] Mennicke C., He M.Y., Clarke D.R. and Smith J.S. The role of secondary oxide inclusions ("PEGS") on the spalling resistance of oxide films. Acta Materialia, 2000, 48, 2941-2949.
[23] Nychka A.J., Clarke D.R. and Meier G.H. Spallation and transient growth on PWA1484 superalloy. Material Science and Engineering A, 2008, 490, 359-368.
[24] Akhtar A., Hegde S. and Reed R.C. The oxidation of single-crystal nickel-based superalloys. JOM Journal of the Minerals, Metals and Materials Society, 2006, 58, 37-42.
[25] Epishin A. and Link T. Mechanisms of high-temperature creep of nickel-based superalloys under low applied stresses. Philosophical Magazine, 2004, 84 (19), 1979-2000.
[26] Ashby M.F. and Dyson B.F. Creep damage mechanics and micromechanisms. Advances in fracture research (Fracture 84). Volume 1 (A86-29951 13- 39). Oxford and New York, Pergamon Press, 1986, 3-30.
[27] Sherry A.H. and Pilkington R. The creep fracture of a single-crystal superalloy. Materials Science and Engineering A, 1993, 173 (1-2), 51-61.
[28] Srivastava A. and Needleman A. Porosity evolution in a creeping single crystal. Submitted to Modelling and Simulation in Materials Science and Engineering, 2011.
[29] Busso E.P., ODowd N.P. and Dennis R.J. A rate dependent formulation for void growth in single crystal materials. IUTAM Sympossium on Creep in Structurees (eds. S. Murakani and N.Ohno), Kluwer Academic Publishers, 2001, 41-50.